Surface-Roughness-Limited Mean Free Path in Si Nanowire FETs

Hyo-Eun Jung and Mincheol Shin

Dept. of Electrical Engineering,
Korea Advanced Institute of Science and Technology, Daejeon 305-732, Rep. of Korea
Email: junghe@kaist.ac.kr, mshin@kaist.ac.kr

***Abstract*—The mean free path (MFP) in silicon nanowire field effect transistors limited by surface roughness scattering (SRS) is calculated with the non-perturbative approach utilizing the non-equilibrium Green's function method. The entrance scattering effect associated with finiteness of the channel length is identified and a method to eliminate it in the calculation of the MFP is developed. The behavior of the MFP with respect to channel length (L), channel width (W), and the root-mean-square (RMS) of the surface roughness is investigated extensively. Our major findings are that the single parameter, RMS/W, can be used as a good measure for the strength of the SRS effects and that the overall characteristics of the MFP are determined by the parameter. In particular, the MFP exponentially decreases with the increase of RMS/W and the MFP versus the gate electric field shows a distinctively different behavior depending on whether the strength of the SRS effects measured by RMS/W is smaller or greater than 0.06.**

***Index Terms*—nanowire, MOSFET, nanowire field effect transistor, quantum transport, mobility, mean free path, surface roughness, non-equilibrium Green's function.**

I. INTRODUCTION

The Si nanowire field effect transistors (SNWFETs) with all around gates have recently emerged as a promising device to replace the conventional planar metal oxide semiconductor field effect transistors (MOSFETs) as the latter face the physical and technological challenges in their scaling-down [1]–[3]. The SNWFETs have the merit of good electrostatic control and hence can deliver high on-state currents. As their overall performance is determined by the aspect ratio of the channel length (L) and channel width (W) [4], it may be desirable to utilize thinner and thinner nanowires. However, rough interfaces between Si and dielectric are unavoidably generated during the fabrication processes, and currents become limited by surface roughness scattering (SRS) as the nanowire cross-sectional size is reduced below 5 nm [5], [6].

The SRS effects in SNWFETs have been a subject of intense theoretical and computational studies. Most of the studies have been performed with the semiclassical approaches such as the Kubo-Greenwood approach [7]–[9], the multi-subband Monte Carlo technique [10], [11], and the direct solution of the one-dimensional Boltzmann transport equation [12], [13]. The Schrodinger-Poisson equations are self-consistently solved in the approaches assuming an infinitely extended homogeneous nanowire, before the nanowire sub-band information is extracted and fed to the semiclassical procedures. There have also been a few studies based the non-equilibrium Green's function (NEGF) method [10], [14]–[19], where coherent electron transport across the channel region with rough Si/dielectric interfaces is considered fully quantum-mechanically. In the non-perturbative approach, the screening effect, electron phase coherence, and the mode mixing effect, among others, are naturally considered whereas these are hard to be implemented directly or disregarded entirely in the semiclassical approaches.

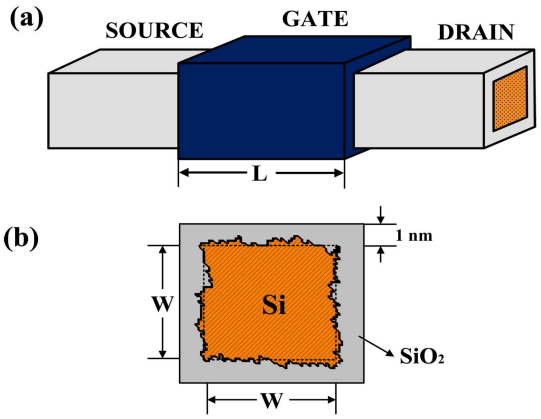

Fig. 1: (a) Schematic diagram of the silicon nanowire field effect transistor with all-around gates. (b) Cross section view at the center of the channel with rough interfaces.

Most of the NEGF studies have so far focused on the low field electron mobility in nanowires. However, the mobility in the device with a finite channel length is not a proper measure for the device performance, because the mobility increases as the channel length increases whereas there should be more detrimental scattering. As Gnani has pointed out, the mean free path (MFP) should be a better indicator of the device performance [20].

In this work, using the non-perturbative NEGF approach, we have for the first time investigated the SR-limited MFP in SNWFETs. Novelty and contributions of this work are: 1) we have devised a systematic way to calculate the MFP in the device with a finite channel length, 2) we have identified the entrance scattering effect which is unavoidable in the device with a source/channel/drain structure, estimated its

strength, and eliminated it from the MFP calculation, and 3) we have thoroughly investigated the behavior of the MFP with a particular emphasis on its dependence on the strength of the SRS effects. These will be discussed in detail in the following sections.

II. Methodology

A. Simulated devices and Hamiltonian

The simulated devices in this work are three-dimensional (3D) rectangular silicon nanowire FETs with all-around gates as shown in Fig. 1. The source and drain regions are heavily n-doped with doping concentration of 10^{20}cm^{-3} whereas the channel is intrinsic. The SiO_2 oxide thickness is assumed to be 1 nm. To describe the electron transport in the conduction band, the effective mass Hamiltonian was used, with the effective masses being scaled according to the tight-binding calculation [21]. All the six equivalent valleys are included in the simulations.

B. Surface roughness generation

The surface roughness (SR) was realized at four Si/SiO_2 interfaces in the channel region only. SR was generated according to the exponentially decaying autocorrelation function expressed as

$$C(\vec{r}) = \Delta_m^2 \exp(-\sqrt{2}r/L_m), \tag{1}$$

where Δ_m is the root-mean square (RMS) fluctuation of the roughness, L_m is the correlation length, and $r = |\vec{r}|$ is the two-dimensional distance between two points on the interface. By Fourier-transforming the autocorrelation function to obtain the power density spectrum (PDS), multiplying a random phase factor to the square root value of PDS, and inverse Fourier-transforming the randomized PDS, instances of rough Si/SiO_2 interfaces were randomly generated [16], [22].

C. NEGF method

We have employed the NEGF method to calculate the charge density and the current in the devices with rough surfaces in the channel region. Self-consistent calculations coupling the charge density from the NEGF equations and the potential from Poisson's equation were carried out. The methodology is well established in the literature [12], [23].

The NEGF procedure with the rough surfaces is the same as the standard non-diffusive calculation procedure. There is no need to calculate the less-than or greater-than Green's functions, because the surface roughness scattering (SRS) is not treated by including the self-energy in the Green's function. Rather, the conduction band edge $E_C(\vec{r})$ at the Si/SiO_2 interfaces is spatially varied in accordance with the generated rough surfaces. In other words, in the Hamiltonian

$$H = H_0 + E_C(\vec{r}) - q_0\phi(\vec{r}), \tag{2}$$

where H_0 is the kinetic part of the Hamiltonian with the inverse effective mass tensor which is not altered by SR,

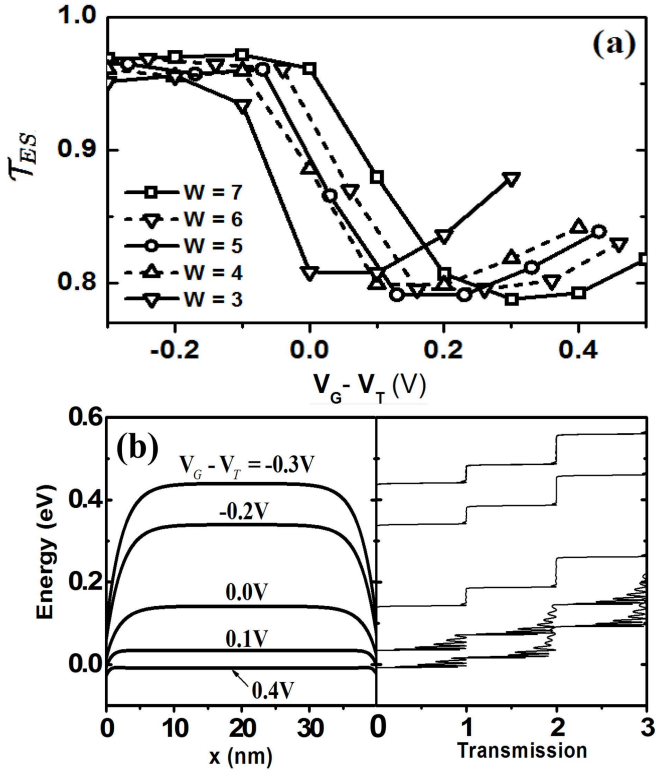

Fig. 2: (a) The effective transmission coefficient $\mathcal{T}_{ES}$ for different wire widths. (b) The conduction-band profiles (1st subband) for different gate voltages and their corresponding transmission functions. Device dimensions are W = 5 nm and L = 40 nm.

$E_C(\vec{r})$ assumes the value of of 0.56 eV or 3.63 eV, if $\vec{r}$ corresponds to silicon or oxide points, respectively. In the Poisson's equation,

$$\overrightarrow{\nabla} \cdot (\epsilon(\vec{r})\overrightarrow{\nabla}\phi(\vec{r})) = q_0(n(\vec{r}) - N_D), \tag{3}$$

$\epsilon(\vec{r})$ is also spatially varying in the same manner as $E_C(\vec{r})$.

In this work, the coupled mode space approach was used [24], [25] with the number of modes ranging from 30 to 50 depending on the cross-sectional width of nanowire. Including higher modes little changed the outcome of the calculations, which validates that the used number of modes is sufficient.

III. Entrance Scattering Effect

In the nanowire FET in Fig. 1, electrons experience quantum mechanical scattering by the channel potential barrier as they enter the channel region. The channel potential barrier is present due to the fact that the source/drain and channel regions are doped with different doping concentrations. The entrance scattering effect (ESE) takes place even in the ballisticity condition (no rough surfaces in the channel region) and should be separated out from the calculated mean free path. The method to isolate the pure contributions from the channel region is elaborated in section IV.

In the nanowire device under consideration, the ballistic

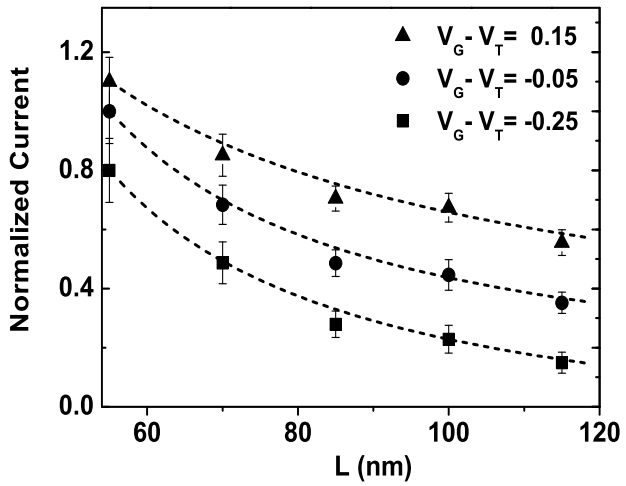

Fig. 3: The drain current versus channel length L for different gate voltages. The currents are normalized by the current of L = 55 nm. Dashed lines are the fit to the function of the form $A/(B+L)$. The curves for $V_G - V_T$ = -0.25 V and 0.15 V are shifted by -0.2 and 0.1, respectively, for a clearer view. Device width and SR parameters are W = 3 nm, Δ_m = 0.3 nm, and L_m = 1.0 nm.

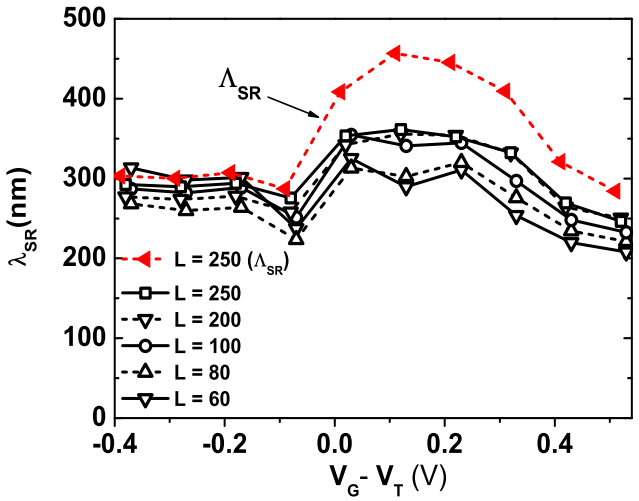

Fig. 4: The mean free path λ_{SR} for different channel lengths. Λ_{SR} as defined in (11) is also displayed. Device width and SR parameters are W = 5 nm, Δ_m = 0.2 nm, and L_m = 1.0 nm.

current I_b can be expressed as, at low V_{DS},

$$I_b = \frac{2q_0^2 V_{DS}}{h} \sum_k \mathcal{T}_k \mathcal{F}_{-1}\left(\frac{E_F - E_k}{k_B T}\right), \tag{4}$$

where $\mathcal{F}_m(x)$ is the m-th order modified Fermi integral, E_k is the energy level of subband k in the channel region, E_F is the Fermi energy, and $\mathcal{T}_k$ is the transmission probability in subband k that accounts for backscattering due to ESE. If the source/drain regions are removed and the same cross-section of the channel region is repeated indefinitely, there is no ESE and $\mathcal{T}_k = 1$ in (4). Let us denote the ballistic current in the infinitely long homogeneous nanowire as $I_{b\infty}$. We write

$$I_b = \mathcal{T}_{ES} I_{b\infty}, \tag{5}$$

where the effective transmission coefficient $\mathcal{T}_{ES}$ is introduced as a measure for the degree of ESE in the nanowire device.

Fig. 2 (a) shows $\mathcal{T}_{ES}$ versus V_G for various W's, where it is shown that $\mathcal{T}_{ES}$ is as low as about 0.8 and its dependence on V_G is not sensitive to W. As shown in Fig. 2 (b), the channel potential barrier is so high in the subthreshold regime that an electron is either completely reflected or completely transmitted depending on whether its energy is below or above the potential barrier, except for a very narrow window of energy located just above the potential barrier where it experiences the quantum-mechanical backscattering. So $\mathcal{T}_{ES}$ is close to 1 in the subthreshold regime. Around V_T, the potential barrier is lowered and at the same time its shape near the ends of the channel becomes sharper so that the quantum mechanical backscattering starts to occur seriously. In other words, the above-mentioned energy window broadens, resulting in a sharp decrease of $\mathcal{T}_{ES}$. If the gate voltage is further increased, $\mathcal{T}_{ES}$ reaches a minima and then slightly increases, because the channel potential barrier is sufficiently lowered to result in lesser backscattering.

IV. MEAN FREE PATH

In devices with finite channel length, the effective mobility is no longer a good indicator of device performance, as it tends to zero as the ballistical condition is approached whereas the ON current increases [20]. Instead, the mean free path (MFP) that is directly related to electron transmission in the device is better suited as the indicator of device performance. In this work, the SR-limited MFP is calculated as follows.

At a low drain bias, we relate I with $I_{b\infty}$ via

$$I = \mathcal{T} I_{b\infty}, \tag{6}$$

where $\mathcal{T}$ is the overall transmission coefficient in the device. $\mathcal{T}$ consists of contributions from the entrance scattering ($\mathcal{T}_{ES}$) and the surface roughness scattering ($\mathcal{T}_{SR}$). In an attempt to isolate $\mathcal{T}_{SR}$, we write

$$\frac{1-\mathcal{T}}{\mathcal{T}} = \frac{1-\mathcal{T}_{ES}}{\mathcal{T}_{ES}} + \frac{1-\mathcal{T}_{SR}}{\mathcal{T}_{SR}}, \tag{7}$$

which is written based on the simple picture that the two sources of scattering are connected serially [26]. Using the defining relationship for the SR-limited MFP λ_{SR},

$$\mathcal{T}_{SR} = \frac{\lambda_{SR}}{\lambda_{SR} + L}, \tag{8}$$

we finally obtain

$$\lambda_{SR} = \frac{L}{\mathcal{T}^{-1} - \mathcal{T}_{ES}^{-1}}. \tag{9}$$

Notice that in defining $\mathcal{T}$ in (6), $I_{b\infty}$ is used instead of I_b. If the relationship $I = \mathcal{T}' I_b$ is used instead of (6), it implies that ESE is disregarded, and we may write

$$\mathcal{T}' = \frac{\Lambda_{SR}}{\Lambda_{SR} + L}. \tag{10}$$

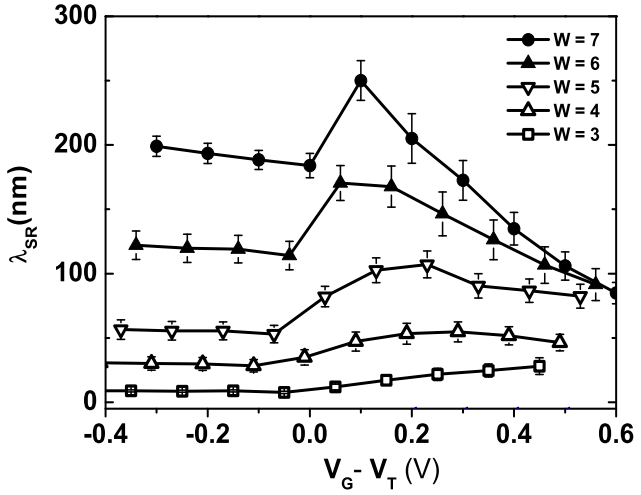

Fig. 5: The mean free path λ_{SR} for different wire widths. The channel lengths were fixed at L = 100 nm for all W's. SR parameters are $\Delta_m = 0.3$ nm and $L_m = 1.0$ nm. Mean value and sample standard deviation (dispersion bars) are reported.

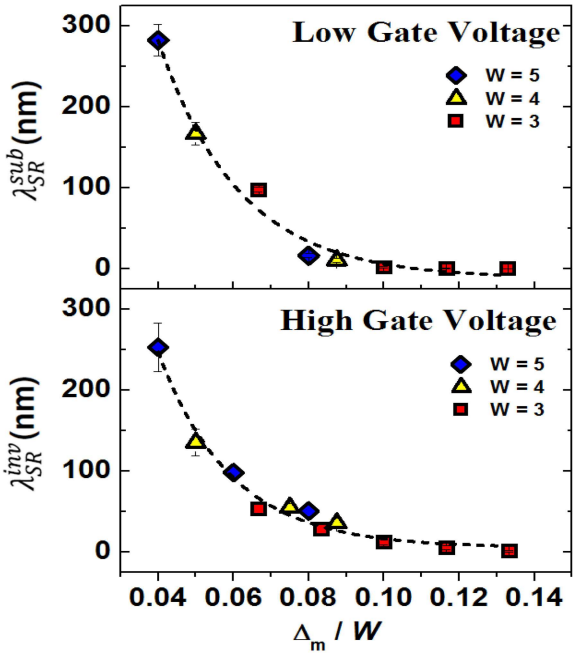

Fig. 6: (Top) The mean free path λ_{SR}^{sub} and (Bottom) λ_{SR}^{inv} evaluated at $V_G - V_T = -0.3$ V and 0.4 V versus Δ_m/W, respectively. Both W and Δ_m were varied and L_m = 1 nm. The data from W = 3, 4, and 5 nm are represented by squares, triangles, and diamonds, respectively. The channel lengths were fixed to 100 nm for all calculations. The dashed lines represent data fit to an exponentially decaying function.

The MFP Λ_{SR} of the above equation is related to λ_{SR} as:

$$\Lambda_{SR} = \frac{1}{\mathcal{T}_{ES}} \lambda_{SR}. \tag{11}$$

That is, the MFP is multiplied by the factor $1/\mathcal{T}_{ES}$, which leads to an unphysical peak as demonstrated below.

Before proceeding further, we first show I as a function of L in Fig. 3, which verifies that diffusive transport expressed by Eqs. (8) or (10) actually takes place due to SR. Note that we have deliberately chosen the device width and the SR parameters in the figure so that resultant MFP is as small as about 10 nm (consult Fig. 7(a)).

Fig. 4 shows thus-calculated λ_{SR} for SNWFETs of $W = 5$ nm. For L varying from 60 nm to 250 nm, λ_{SR} seems to depend on L weakly. The MFP calculated by using (11) is also displayed in the figure: Λ_{SR} shows a pronounced peak around V_T when there is no physical reason for the feature. This supports that λ_{SR} is a more natural choice for the MFP than Λ_{SR}. In the λ_{SR} versus V_G curve of Fig. 4, however, there is still some hint of a peak around V_T. We believe that this is an artifact which is originated from the imperfect nature in the process of isolating the pure SR contribution in the channel region ((7)). As a matter of fact, (7) should hold better for greater L because the assumption that the two sources of scattering (ES and SR) are incoherently connected becomes more valid.

Fig. 5 shows the MFP for different W's when L is fixed at 100 nm. The MFP decreases as W becomes smaller, as expected, but the above-mentioned peaky feature near V_T is more pronounced at larger W. Hereafter let us set aside the unphysical peaky feature near V_T and concentrate on the MFP in the subthreshold region (λ_{SR}^{sub}) and the inversion region (λ_{SR}^{inv}).

Our key findings in this work with regard to the MFP's are: 1) the dimensionless parameter Δ_m/W can be used as a good measure of the SRS strength, 2) the MFP's exponentially decrease with Δ_m/W, and 3) λ_{SR}^{inv} becomes greater than λ_{SR}^{sub} if $\Delta_m/W \gtrsim 0.06$.

Firstly, both λ_{SR}^{sub} and λ_{SR}^{inv} exponentially decrease with Δ_m/W as shown in Fig. 6, where λ_{SR}'s were calculated for all the possible combinations of W = 3, 4, and 5 nm and Δ_m is $0.1 \sim 0.4$ nm. λ_{SR}^{sub} and λ_{SR}^{inv} were evaluated at $V_G - V_T$ = -0.3 V and 0.4 V, respectively. Notice that W is restricted to below 5 nm here. In particular, λ_{SR}^{inv} for $W \geq 5$ nm converges to the almost the same value, as shown in Fig. 5.

The fact that the MFP can be described by a single parameter Δ_m/W, even with different W's, is quite interesting. For the size quantization effects associated with channel width, such as the degree of wave-function confinement, the number of subbands, and the degree of the mixing between subbands, are expected to result in the MFP's dependence on W in a complicate way. Nevertheless, our calculations show the MFP's exponential dependence on Δ_m/W. This should give a useful guide for the estimation of λ_{SR} in Si nanowire devices.

Secondly, we have found that, if the SRS effects become sufficiently strong, λ_{SR} increases with the increase of V_G and, as the consequence, $\lambda_{SR}^{inv} > \lambda_{SR}^{sub}$. This is in sharp contrast to the usual case where λ_{SR} should decrease with the increase of V_G, because more intense scattering is expected to occur at higher gate voltages. In our calculations, the latter is observed for the cases of the SRS effects being relatively weak. See λ_{SR} for W = 5 nm (Δ_m = 0.2 nm) in Fig. 4 and that for W = 6 and 7 nm (Δ_m = 0.3 nm) in Fig. 5, respectively. However, as W becomes smaller in Fig. 5, the usual behavior is not seen

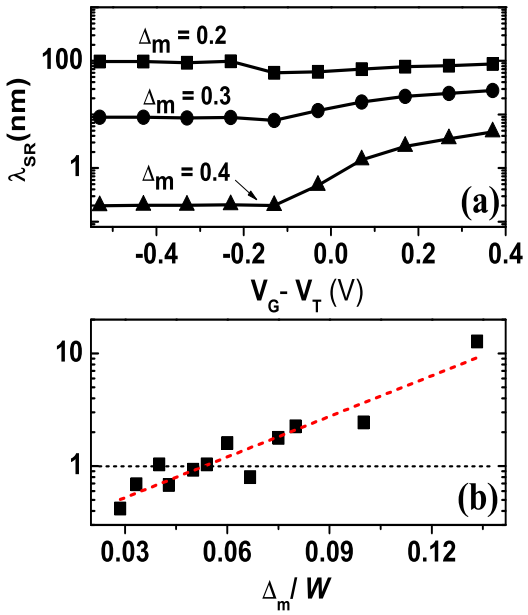

Fig. 7: (a) The mean free path λ_{SR} versus V_G for $W = 3$ nm and $L = 100$ nm, as Δ_m is changed from 0.2 to 0.4 nm and L_m = 1 nm. (b) The ratio $\lambda_{SR}^{inv}/\lambda_{SR}^{sub}$ versus Δ_m/W.

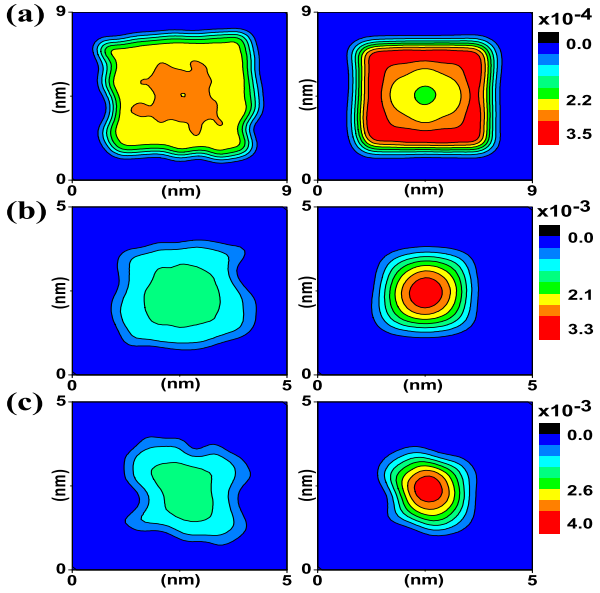

Fig. 8: The cross-sectional electron density profiles for low V_G (left column) and high V_G (right column), for (a) W = 7 nm, $\Delta_m = 0.2$ nm and (b) W = 3 nm, $\Delta_m = 0.2$ nm, and (c) W = 3 nm, $\Delta_m = 0.4$ nm. Electron densities are normalized by the total charge density of the cross-section.

any longer and λ_{SR}^{inv} becomes greater than λ_{SR}^{sub}.

We argue that the ratio $\lambda_{SR}^{inv}/\lambda_{SR}^{sub}$ has to do with the strength of the SRS effects and that Δ_m/W is a good measure for the strength. Obviously, the SRS effects should become stronger as W becomes smaller for fixed Δ_m(case A) or as Δ_m becomes bigger for fixed W(case B). For case A, Δ_m is fixed to 0.3 nm and W is varied as shown in Fig. 5, and we observe that $\lambda_{SR}^{inv}/\lambda_{SR}^{sub}$ becomes bigger than 1 if $\Delta_m/W \geq 0.06$. For case B, W is fixed to 3 nm and Δ_m is varied as shown in Fig. 7 (a). For Δ_m = 0.2 nm in the figure, λ_{SR} already starts to ascend in the inversion regime, although quite slowly. As Δ_m is increased to 0.3 nm and then to 0.4 nm, λ_{SR} ascends more and more steeply and λ_{SR}^{inv} becomes as big as about ten times of λ_{SR}^{sub} for Δ_m = 0.4 nm. (Also compare the curves of W = 5 nm in Fig. 4 and Fig. 5, where Δ_m is changed from 0.2 nm to 0.3 nm.)

If we combine cases A and B and plot $\lambda_{SR}^{inv}/\lambda_{SR}^{sub}$ versus Δ_m/W in Fig. 7 (b), we observe that the ratio $\lambda_{SR}^{inv}/\lambda_{SR}^{sub}$ generally increases with the increase of Δ_m/W, although there are small fluctuations. $\lambda_{SR}^{inv}/\lambda_{SR}^{sub}$ crosses the line of 1 at $\Delta_m/W \sim 0.06$ in the figure. Thus we conclude that the characteristics of the SRS effects in Si nanowires change at $\Delta_m/W \sim 0.06$.

That λ_{SR}^{inv} becomes greater than λ_{SR}^{sub} for the strong SRS effects can be qualitatively explained as follows. In Figs. 8 (b) and (c), the cross-sectional charge densities for the cases of Δ_m = 0.2 and 0.4 nm are compared at low and high gate voltages (W = 3 nm). In the charge density profiles at low gate voltage, the Si/SiO_2 interfaces that fluctuate in proportion to Δ_m can be directly observed. In the charge density profiles at high gate voltage, however, the degree of the interface fluctuations seems to be almost invariant to the increase of the surface roughness. The latter is due to the wave function confinement effect which is of particular importance for nanowires of $W \leq 5$ nm, and consequently, the electrons are concentrated to the center of the nanowire as seen in the figure [4], [16] . Hence the 'effective' surface roughness that felt by the electrons is less at high gate voltage than at low gate voltage. This effect intensifies as Δ_m is increased or W is decreased, resulting in the relationship between $\lambda_{SR}^{inv}/\lambda_{SR}^{sub}$ and Δ_m/W shown in Fig. 7 (b). On the other hand, for nanowires of $W > 5$ nm, the confinement effect is weak so the electrons are pushed to the nanowire surfaces at high gate voltage, resulting in the expected behavior that the MFP decreases with the increase of the gate voltage as shown in Fig. 8 (a).

V. Conclusion

In this work, we have systematically devised the methodology for the calculation of the mean free path in the nanowire field effect transistors with finite channel length. The parasitic entrance scattering effects were identified and carefully eliminated from the MFP calculations. Non-perturbative approach based on the non-equilibrium Green's function method was used to address the SRS effects in the nanowire transistors. The methodology developed in this work can be applied to any scattering mechanism, although only SRS is considered here.

We have found that the SR-limited MFP can be well described by a function which depends on a single parameter Δ_m/W. In particular, the MFP in the subthreshold regime exponentially decreases with the increase of Δ_m/W. For

nanowires of $W \leq 5$ nm, the MFP in the inversion regime also exponentially decreases with Δ_m/W.

We have also found that the dimensionless parameter Δ_m/W can be used as a good measure of the SRS strength. If $\Delta_m/W < 0.06$, one may expect that the SRS effects should be relatively weak, resulting in the usual behavior that the MFP decreases with the increase of the gate electric field. If $\Delta_m/W > 0.06$, on the other hand, the SRS effects can be regarded to be strong, resulting in the extraordinary behavior that the MFP increases with the increase of the gate electric field. Our results should give a useful guide for the estimation of MFP and the strength of the SRS effects in the nanowire devices.

ACKNOWLEDGMENT

This research was supported by the Pioneer Research Center Program and the Basic Science Research Program thorough the National Research Foundation of Korea (NRF) Funded by the Ministry of Education, Science and Technology (Grant No. 2012-0000459 and No. 2012-0002120)

REFERENCES

[1] S. Suk et al.,"High performance 5 nm radius Twin Silicon Nanowire MOSFET(TSNWFET) : Fabrication on Bulk Si Wafer, Characteristics, and Reliability," *IEEE IEDM Electron Devices Meeting*, pp. 717-720, Dec. 2005.

[2] N. Singh et al., "High performance Fully Depleted Silicon Nanowire(Diameter $\leq$ 5nm) Gate-All-Around CMOS Devices," *IEEE Trans. Electron Devices*, vol. 27, pp. 383-386, May 2006.

[3] J. P. Colinge, "Multiple-gate SOI MOSFETs," *Solid State Electron.*, vol. 48, pp. 897-905, June 2004.

[4] M. Shin, "Efficient simulation of silicon nanowire field effect transistors and their scaling behavior," *J. Appl. Phys.*, vol. 101, pp. 024510-1-024510-6, Jan. 2007.

[5] D. Basu, M. J. Gilbert, and S. K. Banerjee, "Surface roughness exacerbated performance degradation in silicon nanowire transistors," *J. Vac. Sci. Technol. B, Microelectron. Process. Phenom.*, vol. 24, pp. 2424-2428, Sep. 2006.

[6] F. Gamiz, J. B. Roldan, J. A. Lopez-Villanueva, P. Cartujo-Cassinello, and J. E. Carceller, "Surface roughness at the Si-SiO_2 interfaces in fully depleted silicon-on-insulator inversion layers," *J. Appl. Phys*, vol. 86, pp. 6854, Sep. 1999.

[7] J. Dura, F. Triozon, S. Barraud, D. Munteanu, S. Martinie, and J. L. Autran, "Kubo-Greenwood approach for the calculation of mobility in gate-all-around nanowire metal-oxide-semiconductor field effect transistors including screened remote Coulomb scattering-comparison with experiment," *J. Appl. Phys.*, vol. 111, pp. 103710-133710-9, May 2012.

[8] S. Jin, M. V. Fischetti, and T. Tang, "Modeling of electron mobility in gated silicon nanowires at room temperature: Surface roughness scattering, dielectric screening, and band nonparabolicity," *J. Appl. Phys.*, vol. 102, pp. 083715-083715-14, Oct. 2007.

[9] S. Barraud, E. Sarrazin, and A. Bournel, "Temperature and size dependences of electrostatics and mobility in gate-all-around MOSFET devices," *Semicond. Sci. Technol.*, vol. 26, pp. 025001, Dec. 2010.

[10] A. Asenov et al., "Simulation of statistical variability in nano-CMOS transistors using drift-diffusion, Monte Carlo and non-equilibrium Green's function techniques," *J. Comput. Electron.*, vol. 8, pp. 349-373, Oct. 2009.

[11] E. B. Ramayya, D. Vasileska, S. M. Goodnick, and I. Knezevic, " Electron Mobility in Silicon Nanowires," *IEEE Trans. Nanotechnology*, vol. 6, pp. 113-117, Jan. 2007.

[12] S. Jin, M. V. Fischetti, and T. Tang, "Theoretical study of carrier transport in silicon nanowire transistors based on the multisubband Boltzmann transport equation," *IEEE Trans. Electron Devices*, vol. 55, pp. 2886-2897, Nov. 2008.

[13] M. Lenzi, A. Gnudi, S. Reggiani, E. Gnani, M. Rudan, and G. Baccarani, "Semiclassical transport in silicon nanowire FETs including surface roughness," *J. Comput. Electron.*, vol. 7, pp. 355-358, Sep. 2008.

[14] K. Rogdakis, S. Poli, E. Bano, K. Zekentes, and M. G. Pala, "Phonon- and surface-roughness-limited mobility of gate-all-around 3C-SiC and Si nanowire FETs," *Nanotechnology*, vol. 20, pp. 295202, July 2009.

[15] J. Wang, E. Polizzi, A. Ghosh, S. Datta, and M. Lundstrom, "Theoretical investigation of surface roughness scattering in silicon nanowire transistors," *Appl. Phys. Lett.*, vol. 87, pp. 043101-1-043101-3, July 2005.

[16] S. Poli, M. G. Pala, T. Poiroux, S. Deleonibus, and G. Baccarani, "Size dependence of surface-roughness-limited mobility in silicon nanowire," *IEEE Trans. Electron Devices*, vol. 55, pp. 2968-2976, Nov. 2008.

[17] C. Buran, M. G. Pala, M. Bescond, M. Dubois, and M. Mouis, "Three-dimensional real-space simulation of surface roughness in silicon nanowire FETs," *IEEE Trans. Electron Devices*, vol. 56, pp. 2186-2192, Oct. 2009.

[18] A. Martinez, "Variability in Si Nanowire MOSFETs Due to the Combined Effect of Interface Roughness and Random Dopants: A Fully Three-Dimensional NEGF Simulation Study," *IEEE Trans. Electron Devices.*, vol. 57, pp. 1626-1635, July 2010.

[19] S. G. Kim, M. Luisier, A. Paul, T. B. Boykin, and G. Klimeck, "Full Three-Dimensional Quantum Transport Simulation of Atomistic Interface Roughness in Silicon Nanowire FETs," *IEEE Trans. Electron Devices*, vol. 58, pp. 1371-1380, May 2011.

[20] E. Gnani, A. Gnudi, S. Reggiani, and G. Baccarani, "Effective mobility in nanowire FETs under quasi-ballistic conditions," *IEEE Trans. Electron Devices*, vol. 57, pp. 336-344, Jan. 2010.

[21] J. Wang, A. Rahman, A. Ghosh, G. Klimeck, and M. Lundstrom, "On the validity of the parabolic effective mass approximation for the I-V calculation of silicon nanowire transistors," *IEEE Trans. Electron Devices*, vol. 52, pp. 1589-1595, July 2005.

[22] S. M. Goodnick, D. K. Ferry, and C. W. Wilmsen, "Surface roughness at the Si(100)-SiO_2 interface," *Phys. Rev. B*, vol. 32, pp. 8171-8185, Dec. 1985.

[23] M. Shin, "Quantum simulation of device characteristics of Silicon nanowire FETs," *IEEE Trans. Nanotechnology*, vol. 6, pp. 230-237, Mar. 2007.

[24] M. Luisier, A. Schenk, and W. Fichtner, "Quantum transport in two- and three-dimensional nanoscale transistors: Coupled mode effects in the nonequilibrium Green's function formalism," *J. Appl. Phys.*, vol. 100, pp. 043713, Aug. 2006.

[25] J. Wang, E. Polizzi, and M. Lundstrom, "A three-dimensional quantum simulation of silicon nanowire transistors with the effective-mass approximation," *J. Appl. Phys.*, vol. 96, pp. 2192, May. 2004.

[26] S. Datta, "Electronic transport in mesoscopic systems," *Cambridge university Press*.